Influence of Aging, Thermal, Hydrothermal, and Mechanical Treatments on the Porosity of MCM-41 Mesoporous Silica

ARTICLE *in* LANGMUIR · MAY 2002

Impact Factor: 4.46 · DOI: 10.1021/la0118255

6 AUTHORS, INCLUDING:

Sabine Valange
Université de Poitiers
80 PUBLICATIONS **752** CITATIONS
SEE PROFILE

Jean-Pierre Bellat
University of Burgundy
109 PUBLICATIONS **1,159** CITATIONS
SEE PROFILE

Guy Weber
University of Burgundy
50 PUBLICATIONS **396** CITATIONS
SEE PROFILE

Gabelica Zelimir
Chinese Academy of Sciences
219 PUBLICATIONS **3,714** CITATIONS
SEE PROFILE

Influence of Aging, Thermal, Hydrothermal, and Mechanical Treatments on the Porosity of MCM-41 Mesoporous Silica

M. Broyer,[†] S. Valange,[‡,§] J. P. Bellat,*[,†] O. Bertrand,[†] G. Weber,[†] and Z. Gabelica[‡]

Laboratoire de Recherches sur la Réactivité des Solides - UMR 5613 CNRS, Université de Bourgogne - UFR ST, 9 allée A. Savary, BP 47870 - F-21078 Dijon Cedex, France, and Groupe Sécurité et Ecologie Chimiques, ENSCMu, Université de Haute Alsace, 3 rue Alfred Werner, F-68093 Mulhouse Cedex, France

Received December 18, 2001. In Final Form: April 1, 2002

A mesoporous siliceous material of MCM-41 type was characterized by nitrogen adsorption, X-ray diffraction, and Fourier transform infrared spectroscopy. Its pore diameter, external and internal surface, pore volume, wall thickness, and pore wall density were determined. Special attention was paid to sample aging and its stability toward temperature, water vapor, and mechanical compression, aiming at using this material in industrial applications such as adsorption or catalysis. Calcined MCM-41 loses an important part of its mesoporosity during aging under ambient temperature, pressure, and humidity conditions but then becomes stable after 3 months, still retaining a noticeable porosity. The aged MCM-41 can withstand temperatures up to 873 K and uniaxial compressions up to 100 MPa without too much damage. After contact with water vapor at 358 K, the porous structure was totally destroyed and an amorphous phase was obtained.

Introduction

Porous solids are used technically as adsorbents, catalysts, and catalyst supports owing to their high surface areas and noticeable pore volumes. Although zeolites, which belong to the microporous class, provide very good catalytic and adsorption properties, their applications at an industrial level are sometimes limited by their relatively small pore openings. A growing interest was therefore devoted to mesoporous materials with the aim to extend the field of catalysis and adsorption to large molecules. The MCM-41 material (Mobil Composition of Matter), a member of the M41S mesoporous silica family discovered in the early 1990s by the Mobil Oil Corp.,[1] is subject to extended research, often oriented to physical and chemical engineering applications. Indeed, with its parallel cylindrical pores arranged in a hexagonal lattice (Figure 1) and a pore radius ranging from 2 to about 30 nm, this material made of amorphous silica is a model porous solid particularly well adapted for adsorption and catalytic reactions involving large molecules. Most of the research on this material was devoted to its synthesis pathways and characterization of its porosity and surface properties. The specific papers published in this field being too numerous to be quoted, we will restrict to mention a nonexhaustive list of the most recent review papers on the subject where most of such references are cited.[2]

Concerning the physicochemical characteristics of mesoporous materials, it appears that the pore characteristics (pore radius, specific surface area, pore volume, etc.) are strongly dependent not only on the synthesis procedures or on postsynthesis treatments (calcination, pelletization, etc.) but also on the experimental techniques used to characterize these properties. Several researchers[3−8] have used MCM-41 as a model porous solid to check the different methods of pore characterization included in the software

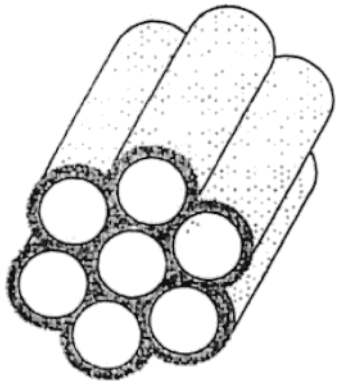

Figure 1. Schematic representation of the pore network of MCM-41.

* To whom correspondence should be addressed. E-mail: jean-pierre.bellat@u-bourgogne.fr. Phone: (33) 03 80 39 59 29. Fax: (33) 03 80 39 61 32.

[†] Université de Bourgogne.

[‡] Université de Haute Alsace.

[§] Present address: LACCO, UMR CNRS 6503, ESIP, 40 avenue du Recteur Pineau, F-86022 Poitiers Cedex, France.

(1) Kresge, C. T.; Leonowicz, M. E.; Roth, W. J.; Vartuli, J. C.; Beck, J. S. *Nature* **1992**, *359*, 710.

(2) See, for example: Sayari, A.; Liu, P. *Microporous Mater.* **1997**, *12*, 149. Corma, A. *Top. Catal.* **1997**, *4*, 249. Stucky, G. D.; Huo, Q.; Firouzi, A.; Chmelka, B. F.; Schacht, S.; Voigt-Martin, I. G.; Schüth, F. *Stud. Surf. Sci. Catal.* **1997**, *105A*, 3. Ying, J. Y.; Mehnert, C. P.; Wong, M. S. *Angew. Chem., Int. Ed. Engl.* **1999**, *38*, 56. Ciesla, U.; Schüth, F. *Microporous Mesoporous Mater.* **1999**, *27*, 131. Selvam, P.; Bhatia, S. K.; Sonwane, C. G. *Ind. Eng. Chem. Res.* **2001**, *40*, 3237.

(3) Ravikovitch, P. L.; Domhnaill, S. C. O.; Neimark, A. V.; Schüth, F.; Unger, K. K. *Langmuir* **1995**, *11*, 4765.

(4) Lastoskie, C.; Gubbins, K. E.; Quirke, N. *J. Phys. Chem.* **1993**, *97*, 4786.

(5) Kruk, M.; Jaroniec, M.; Sayari, A. *J. Phys. Chem. B* **1997**, *101*, 583.

(6) Zhu, H. Y.; Zhao, X. S.; Lu, G. Q.; Do, D. D. *Langmuir* **1996**, *12*, 6513.

(7) Sayari, A.; Liu, P.; Kruk, M.; Jaroniec, M. *Chem. Mater.* **1997**, *9*, 2499.

(8) Kruk, M.; Antochshuk, V.; Jaroniec, M. *J. Phys. Chem.* **1999**, *103*, 10670.

10.1021/la0118255 CCC: $22.00
Published on Web 05/31/2002

of current commercial sorption instruments for the application of the Brunauer−Emmett−Teller (BET) theory, the comparison methods (*t*-plot, α_s-plot), and the methods based on the Kelvin equation. Galarneau et al.[9] have published a critical review on comparative tests of mesopore size evaluation methods. They show that the use of such methods for the determination of the pore radius is sometimes questionable and leads, in some cases, to an underestimation of the pore radius. The major failure of the classical methods of pore characterization such as BET, *t*-plot, or Kelvin equation lies in the selection of the values describing the physical properties of the molecular nitrogen probe. Indeed, it is usually admitted that the nitrogen adsorbed at 77 K behaves like a liquid whereas the nitrogen interacting with pore walls could have a different behavior. The chemical nature and the surface curvature may largely influence the physical properties of nitrogen such as, for example, its cross-sectional area, its density, or its surface tension. The nonlocal density functional theory (NLDFT), extensively developed by Neimark et al.[3,10−12] in the past five years, appears as the more accurate way to characterize the pore size distribution in microporous and mesoporous materials. Moreover, this new approach gives valuable information about the capillary condensation phenomenon in the mesopores, which still remains poorly understood. However, this complex method is not yet widely used and is only reserved to the specialists in the field of the NLDFT. On the other hand, an accurate evaluation of the pore wall density still arouses a keen interest. Indeed, its determination is very delicate and hence widely differs from one work to another, for the same material.

In addition, the behavior of MCM-41, when submitted for a long time to particular conditions of temperature, water vapor pressure, or mechanical constraints, conditions that actually occur during industrial applications, has not been extensively studied so far. While the resistance of MCM-41 in basic or acidic solutions was recently subjected to a series of systematic investigations,[13−22] postsynthesis thermal, hydrothermal, or mechanical properties of such materials are less well documented.[15,18,19,22−27]

The present work is devoted to an in-depth characterization of the porosity, pore wall thickness, and density of a typical Si−MCM-41 fully calcined sample, by combining several techniques such as helium pycnometry, nitrogen adsorption, X-ray diffraction, and Fourier transform infrared (FTIR) spectroscopy. The pore radius and the wall thickness were determined by using and critically comparing the three classical methods of pore evaluation (BET, *t*-method, and Kelvin equation) but by carefully choosing the values of the physical characteristics of the molecular probe such as the cross-sectional area and the surface tension, as suggested in the literature.

In a second step, special attention has been paid to the evaluation of the stability of that material under ambient conditions (aging). Finally, the mechanical, thermal, and hydrothermal stabilities of the aged material were tested under conditions that may occur during their industrial use in catalysis or adsorption.

Experimental Section

The MCM-41 mesoporous silica was synthesized in classical alkaline media using conventional literature recipes.[21,28] Typically, solid cetyltrimethylammonium bromide (CTMABr) is dissolved in NaOH solution, to which a tetramethyl orthosilicate (TMOS) solution is then added dropwise. The final pH, stabilized to about 12.5, was decreased and adjusted at 10.5 by slowly adding a diluted HNO_3 solution. The molar gel composition is the following: 1 SiO_2, 0.215 CTMABr, 1 NaOH, and 125 H_2O. The heavy precipitate that quasi instantaneously appears is homogenized by vigorous stirring for 1 h at ambient temperature and then heated at 383 K in a Teflon-coated stainless steel autoclave for 24 h, under autogenous pressure. The white precipitate was filtered, washed with cold water, and dried at 353 K overnight. The as-synthesized sample was calcined under an air flow in order to remove the surfactant molecules ($CTMA^+$ ions) occluded in the pore system of the mesoporous silica. It was first heated to 473 K at a rate of 1 K min^{-1} and kept for 2 h at that temperature prior to further heating to 873 K at a rate of 1 K min^{-1}. It was finally held at that temperature for another 4 h. Such mild heating conditions are recommended in order to prevent an extensive local heating of the material (generation of hot spots) upon the oxidative surfactant decomposition. The sample obtained after this treatment will be referred to as MCM-41 A. Part of this sample was then allowed to age under ambient temperature and humidity conditions by simply being left stored in a glass bottle. The resulting sample obtained after 3 months of aging will be referred to as MCM-41 B.

Nitrogen adsorption was carried out at 77 K on about 150 mg of sample using a stainless steel homemade manometric apparatus. Prior to each adsorption measurement, the sample was either purged by a nitrogen flow at room temperature or outgassed overnight in situ at 523 K under a vacuum of 10^{-5} hPa. The isothermally adsorbed amounts, expressed as the volume of liquid nitrogen (ρ = 0.8081 g cm^{-3} at 77 K) adsorbed per gram of adsorbent activated at 523 K, were plotted versus the relative pressure p/p_0 (p_0 = 101 325 Pa). X-ray powder diffraction (XRD) patterns were recorded at room temperature on a diffractometer equipped with an INEL curved counter by using Cu Kα radiation. The IR spectra were obtained on a Perkin-Elmer 1725X FTIR spectrometer. The FTIR spectra were recorded at room temperature using KBr-supported wafers in the range 4000−400 cm^{-1}, at a resolution of 4 cm^{-1}. The density of the materials was measured with helium at 298 K in the same manometric apparatus used for nitrogen adsorption.[29] The helium was previously dehydrated by means of a cryogenic trap (liquid nitrogen), and the measurements were performed at low pressure

(9) Galarneau, A.; Desplantier, D.; Dutartre, R.; Di Renzo, F. *Microporous Mesoporous Mater.* **1999**, *27*, 297.
(10) Neimark, A. V.; Ravikovitch, P. I. *Langmuir* **1997**, *13*, 5148.
(11) Ravikovich, P. I.; Haller, G. L.; Neimark, A. V. *Adv. Colloid Interface Sci.* **1998**, *76−77*, 203.
(12) Schumacher, K.; Ravikovitch, P. I.; Du Chesne A.; Neimark, A. V.; Unger, K. K. *Langmuir* **2000** *16*, 4648.
(13) Bellat, J. P.; Bertrand, O.; Bouvier, F.; Broyer, M.; François, V.; Maure, S.; Weber, G. *Stud. Surf. Sci. Catal.* **1999**, *125*, 737.
(14) Zhao, X. S.; Lu, G. Q.; Millar, G. J. *Ind. Eng. Chem. Res.* **1996**, *35*, 2075.
(15) Chen, L. Y.; Janiecke, S.; Chuah, G. K. *Microporous Mater.* **1997**, *12*, 323.
(16) Choudhary, V. R.; Sansare, S. D. *Proc.—Indian Acad. Sci., Chem. Sci.* **1997**, *109*, 229.
(17) Kim, J. M.; Ryoo, R. *Bull. Korean Chem. Soc.* **1996**, *17*, 66.
(18) Trong On, D.; Zaidi, S. M. J.; Kaliaguine, S. *Microporous Mesoporous Mater.* **1998**, *22*, 211.
(19) Landau, M. V.; Varkey, S. P.; Herskowitz, M.; Regev, O.; Pevzner, S.; Sen, T.; Luz, Z. *Microporous Mesoporous Mater.* **1999**, *33*, 149.
(20) Van Bekkum, H.; Kloetstra, K. R. *Stud. Surf. Sci. Catal.* **1998**, *117*, 171.
(21) Noda Perez, C.; Moreno, E.; Henriques, C. A.; Valange, S.; Gabelica, Z.; Monteiro, J. L. F. *Microporous Mesoporous Mater.* **2000**, *41*, 137.
(22) Corma, A.; Fornes, V.; Navarro, M. T.; Perez-Pariente, J. *J. Catal.* **1996**, *159*, 375.
(23) Gabelica, Z.; Valange, S.; Shibata, M.; Hotta, H.; Suzuki, T. *Microporous Mesoporous Mater.* **2001**, *44−45*, 645.
(24) Wu, J.; Liu, X.; Tolbert, S. H. *J. Phys. Chem. B* **2000**, *104*, 11837.
(25) Galarneau, A.; Desplantier-Giscard, D.; Di Renzo, F.; Fajula, F. *Catal. Today* **2001**, *68*, 191.
(26) Di Renzo, F.; Testa, F.; Chen, J. D.; Cambon, H.; Galarneau, A.; Plee, D.; Fajula, F. *Microporous Mesoporous Mater.* **1999**, *28*, 437.
(27) Gusev, V. Y.; Feng, X.; Bu, Z.; Haller, G. L.; O'Brien, J. A. *J. Phys. Chem.* **1996**, *100*, 1985.
(28) Van den Bossche, G.; Sobry, R.; Fontaine, F.; Clacens, J. M.; Gabelica, Z. *J. Appl. Crystallogr.* **1997**, *30*, 1065.
(29) Broyer, M. Ph.D. Thesis, Université de Bourgogne, Dijon, France, 2001.

Table 1. Pore Radius (Rp) of the MCM-41 Samples A and B, Purged under Nitrogen Flow at Room Temperature, Derived from Nitrogen Adsorption Measurements, X-ray Diffraction, and Helium Pycnometry, by Using Different Methods[a]

method	parameter	MCM-41 A	MCM-41 B
X-ray diffraction + He pycnometry + N_2 adsorption	d/g cm^{-3}	2.41 ± 0.12	2.40 ± 0.10
	a/nm	4.6	4.08
	Vp_{cc}/cm^3 g^{-1}	0.822	0.445
	$(p/p_0)_{cc}$	0.86	0.90
	Rp/nm	1.97	1.54
	e/nm	0.66	1.00
N_2 adsorption + BET + $2V/S$	S_{BET}/m^2 g^{-1}	805 ± 8	547 ± 6
	Rp/nm	2.04	1.63
N_2 adsorption + t-method + $2V/S$	St/m^2 g^{-1}	827 ± 17	537 ± 11
	Sext/m^2 g^{-1}	36 ± 2	60 ± 6
	Sp/m^2 g^{-1}	791	477
	Vp/cm^3 g^{-1}	0.765	0.376
	Rp/nm	1.93	1.58
corrected Kelvin eq	$(p/p_0)_{step}$	0.32−0.39	0.15−0.31
	Rp(K)/nm	2.09	1.66

[a] d, pore wall density measured by helium pycnometry; a, lattice parameter; Vp_{cc}, mesopore volume taken on the nitrogen adsorption isotherm at $(p/p_0)_{cc}$; $(p/p_0)_{cc}$, relative pressure at which interparticle capillary condensation starts; e, pore wall thickness; S_{BET}, specific surface area determined by BET analysis; St, total surface determined from the t-plot; Sext, external surface area determined from the t-plot; Sp = St − Sext, mesopore (internal) surface; Vp, mesopore volume determined from the t-plot; $(p/p_0)_{step}$, relative pressure range corresponding to the extent of the step; Rp(K), pore radius derived from the maximum of the pore size distribution curve given by the corrected Kelvin equation.

in the range of 10^{-4}−10 hPa after outgassing the sample at room temperature under vacuum. The mass of sample was 1 g, and the statistical accuracy in density measurements, as estimated by measuring the density of a pure silica (Aerosil 200, $\rho = 2.20$ g cm^{-3}), does not exceed 0.15 g cm^{-3}.

Results and Discussion

Characterization of the Freshly Calcined Material MCM-41 A. The pore wall density measured by helium pycnometry is in good agreement with the usual density of amorphous silica, $d_{SiO_2} = 2.20$ g cm^{-3} (Table 1). Other measurements performed with nitrogen at 500 K in order to avoid any adsorption on the surface give a pore wall density of 2.50 g cm^{-3}. Despite the fact that Floquet et al.[30] and Edler et al.[31] found lower values, there is now no doubt that the pore wall density is the same as for pure silica. The value of 2.20 g cm^{-3}, which is taken for the MCM-41 density in most of the experimental works, is then quite justified, as also supported by Kruk and Jaroniec[32] and Di Renzo et al.[26]

The X-ray diffraction pattern of MCM-41 A is shown in Figure 2. The observation of four peaks at very small angles (2−8° 2θ), which can be indexed in a hexagonal lattice and correspond well to the hexagonally arranged pore structure of MCM-41, is the proof of a long-range order and consequently of a good quality of our sample. As the material is not crystalline at the atomic level, no reflections at higher angles are observed. The lattice parameter $a = d_{100}(2/3^{1/2})$ is a measure of the average distance between

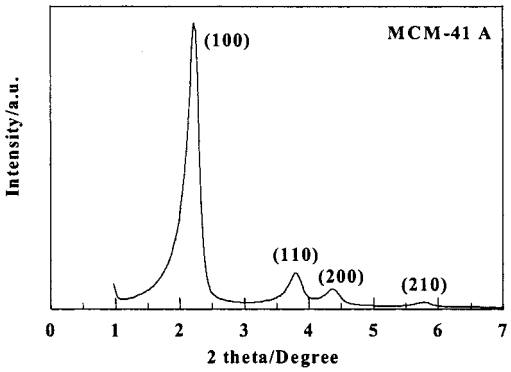

Figure 2. X-ray diffraction pattern of freshly calcined MCM-41 (sample A).

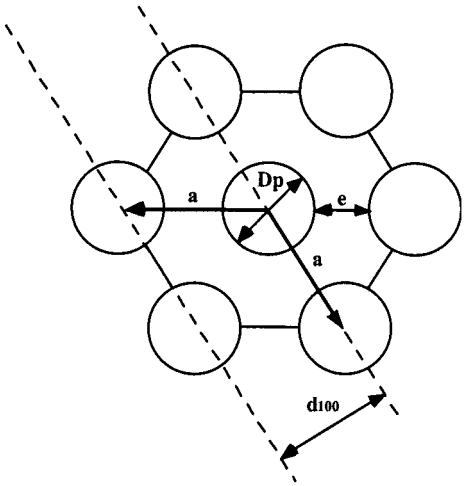

Figure 3. Schematic representation of the hexagonal lattice of MCM-41 in the (001) plane.

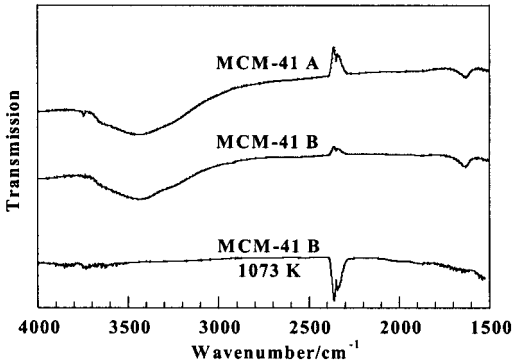

Figure 4. FTIR spectra in the 4000−1500 cm^{-1} region of MCM-41 samples A and B and after thermal treatment at 1073 K under vacuum of sample B.

the two neighboring pore centers in the MCM-41 structure, d_{100} being the XRD interplanar spacing of the first diffraction peak (Figure 3). The value of the lattice parameter given in Table 1 is in good agreement with the transmission electronic microscopic observations.[28]

The FTIR spectra of MCM-41 A (Figures 4 and 5) exhibit a broad absorption band located in the 3700−2700 cm^{-1} interval and are easily assigned to hydrogen-bonded Si−OH groups with adsorbed water. The weak IR absorption band at 3738 cm^{-1} is ascribed to single and geminal Si−OH groups. The typical band at 1636 cm^{-1} representative of adsorbed water (OH bending) is also observed. Bands ranging from 1400 to 400 cm^{-1} arise from fundamental lattice vibrations. The vibration band at 1093 cm^{-1} is attributed to asymmetric Si−O−Si stretching vibrations

(30) Floquet, N.; Coulomb, J. P.; Giorgio, S.; Grillet, Y.; Llewellyn, P. L. *Stud. Surf. Sci. Catal.* **1998**, *117*, 583.
(31) Edler, K. J.; Reynolds, P. A.; White, J. W.; Cookson, D. *J. Chem. Soc., Faraday Trans.* **1997**, *93* (1), 199.
(32) Kruk, M.; Jaroniec, M. *Chem. Mater.* **1999**, *11*, 492.

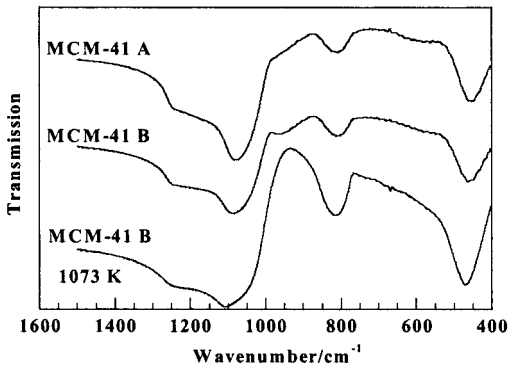

Figure 5. FTIR spectra in the 1500−400 cm^{-1} region of MCM-41 samples A and B and after thermal treatment at 1073 K under vacuum of sample B.

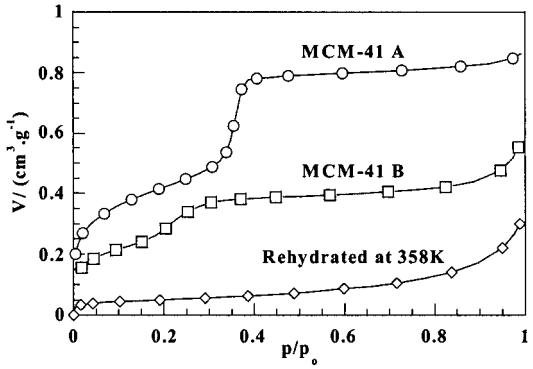

Figure 6. Adsorption isotherms of N_2 at 77 K on freshly calcined MCM-41 (sample A), after 3 months aging (sample B), and after hydrothermal treatment of sample B at 358 K.

(intertetrahedral mode), while those at 806 and 466 cm^{-1} correspond to symmetric O−Si−O stretching vibrations and the O−Si−O bending mode, respectively (intratetrahedral modes).[33,34] A shoulder of weak intensity close to 960 cm^{-1} is attributed to the OH bending of the Si−OH groups.[35]

The nitrogen adsorption isotherm for MCM-41 A activated under nitrogen is shown in Figure 6. This sample exhibits a type IV isotherm in the IUPAC classification[4,36] with a sharp step over a narrow range of relative pressure arising from the condensation of nitrogen inside the primary mesopores. No adsorption−desorption hysteresis was observed. The nitrogen adsorption data were analyzed by the BET theory.[5] The specific surface area (S_{BET}) is calculated by taking for nitrogen cross-sectional area the value of 0.135 nm^2, as proposed by Jelinek et al.[37] (Table 1). Indeed, these authors have shown that in the particular case of nitrogen adsorbed on hydrated silicon dioxide surfaces, it is better to use this value rather than 0.162 nm^2, currently used for hydrated silicon dioxide surfaces.

The relatively small value of S_{BET} obtained, namely, 805 $m^2\ g^{-1}$, is probably due to the fact that the sample was only activated under nitrogen flow, without heating. When the very same sample was outgassed at 350 °C under vacuum ($p = 2 \times 10^{-3}$ hPa) for 4 h prior to the adsorption

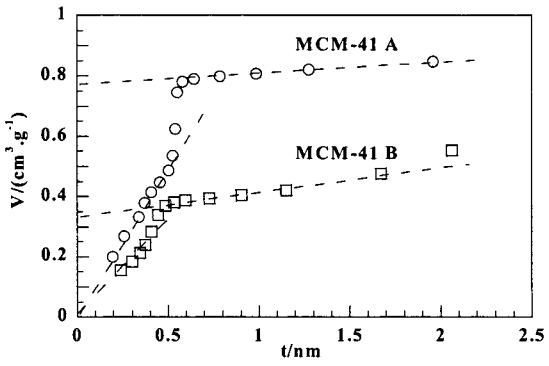

Figure 7. *t*-Plot for the adsorption of N_2 at 77 K on MCM-41 A and B activated at 523 K.

experiment, its S_{BET} was 1190 $m^2\ g^{-1}$.[38] This value is comparable to the one measured on a sample prepared under similar conditions and involving a similar pore wall thickness, outgassed at 250 °C under vacuum ($p = 3 \times 10^{-3}$ hPa), namely, 1190 $m^2\ g^{-1}$. These differences can be rationalized by considering that the evacuation under nitrogen flow and room temperature would not readily eliminate much of the superficial silanol groups (up to 5 SiOH per nm^2 [39]), that at least cover the hydrophilic flat sides of the pores of the mesophase.[26] Most of such silanols start to disappear from a silicon dioxide surface when mild temperatures (200−300 °C) and mild vacuum (ca 10^{-3} hPa) are applied.[26,39]

The nitrogen adsorption data were also analyzed with the *t*-method of Lippens and de Boer.[40] The *t*-plot was drawn using a hydroxylated silica (Aerosil 200) as a nonporous reference adsorbent (Figure 7). Three distinct linear stages are observed in the *t*-plots as defined by Branton et al.:[41] the first one corresponds to the adsorption on the external surface and on the mesopore internal surface, the second one to the reversible condensation in the mesopores, and the last one to the multilayer adsorption on the external surface. This last linear stage also takes into account an additional phenomenon, namely, the compression of the fluid condensed in the mesopores, which takes place after condensation. This effect leads to an overestimation of the external surface area but, as remarked by Kruk et al.,[5] is not likely to cause a significant relative error in the primary mesopore volume and surface area when the external surface area is small. By neglecting this effect, values of the pore volume (Vp), the external surface area (Sext), the total surface area (St), and the pore surface area (Sp) are derived from this plot and reported in Table 1. St was estimated from the slope of the *t*-plot in the monolayer region at low p/p_0; the values of Sext and Vp were determined from the slope and the zero intercept of the multilayer section at high p/p_0, respectively. Sp was calculated using the relationship Sp = St − Sext. It was assumed that the kinetic diameter of the nitrogen molecule was 0.364 nm and that the adsorbate had the liquid nitrogen normal density at 77 K (0.8081 g cm^{-3}). No indication of any primary micropore filling by nitrogen was observed since the linear initial section of the *t*-plot can be back-extrapolated to the origin.

(33) Zhao, X. S.; Lu, G. Q.; Whittaker, A. K.; Millar, G. J.; Zhu, H. Y. *J. Phys. Chem. B* **1997**, *101*, 6525.
(34) Landmesser, H.; Kosslick, H.; Storek, W.; Fricke, R. *Solid State Ionics* **1997**, *101−103*, 271.
(35) Brinker, C. J.; Scherer, G. W. *Sol−Gel Science*; Academic Press: Boston, 1990; p 908.
(36) Sing, K. S. W.; Everett, D. H.; Haul, R. A. W.; Moscou, L.; Pierotti, R. A.; Rouquerol, J.; Siemieniewska, T. *Pure Appl. Chem.* **1985**, *57*, 603.
(37) Jelinek, L.; Kovats, E. *Langmuir* **1994**, *10*, 4225.
(38) Valange, S. Ph.D. Thesis, University of Mulhouse, Mulhouse, France, 2000.
(39) Iler, R. K. *The Chemistry of Silica*; Wiley: New York, 1979; p 866.
(40) De Boer, J. H.; Lippens, B. C.; Linsen, B. G.; Broekhoff, J. C. P.; Van den Heuel, A.; Osinga, Th. J. *J. Colloid Interface Sci.* **1966**, *21*, 405.
(41) Branton, P. J.; Sing, K. S. W.; White, J. W. *J. Chem. Soc., Faraday Trans.* **1997**, *93*, 2337.

The mean pore radius has been calculated with three different methods: the geometric method, the $2V/S$ method, and the Kelvin equation.

Geometric Method. This method, which requires X-ray, helium pycnometry, and nitrogen adsorption data, is recognized as the most accurate way to evaluate the mesopore mean radius. Assuming a perfect cylindrical geometry of the mesopores arranged in a hexagonal lattice, the pore radius can be calculated by the relation[9]

$$\mathrm{Rp} = 0.5515a\sqrt{\frac{\mathrm{Vp_{cc}}}{\mathrm{Vp_{cc}} + \frac{1}{d}}} \qquad (1)$$

where a is the pore lattice parameter, d is the pore wall density, and $\mathrm{Vp_{cc}}$ is the mesopore volume taken on the plateau of the adsorption isotherm at the relative pressure $(p/p_0)_{cc}$ at which starts the capillary condensation of nitrogen between the solid particles, after compression of the condensed fluid phase.

2V/S Method. Assuming that the pores are nonintersecting cylindrical capillaries, the radius of a pore is related to its volume and surface by the relation $R = 2V/S$. The mean pore radius has been calculated by taking for V and S either $\mathrm{Vp_{cc}}$ and S_{BET} given by the adsorption isotherm and the BET model, respectively, or Vp and Sp deduced from the t-plot. The first way takes into account the compression of the fluid phase adsorbed in the mesopores, while the second takes into account the external surface.

Corrected Kelvin Equation. The pore size distribution is usually determined by the application of the Kelvin equation[42] in the range of relative pressures p/p_0 for which capillary condensation occurs:

$$\mathrm{Rk}(p/p_0) = \frac{2\gamma_\infty V_\mathrm{L}}{RT\,Ln(p_0/p)} \qquad (2)$$

with the ideal gas constant $R = 8.314$ J K^{-1} mol^{-1}, the surface tension $\gamma = 8.72 \times 10^{-3}$ N m^{-1}, and the molecular volume $V_\mathrm{L} = 34.68$ cm^3 mol^{-1} for nitrogen at $T = 77$ K. $\mathrm{Rk}(p/p_0)$ is the core radius determined using eq 2 at a given p/p_0 value. Assuming perfect wettability of nitrogen on the surface, that is, a contact angle $\theta = 0$, the pore radius $\mathrm{Rp}(p/p_0)$ is related to the core radius $\mathrm{Rk}(p/p_0)$ by the relation

$$\mathrm{Rp}(p/p_0) = \mathrm{Rk}(p/p_0) + t \qquad (3)$$

where t is the statistical thickness of the layer adsorbed on the nonporous silica (Aerosil 200). It is well-known that the Kelvin equation underestimates the pore radius.[3,9,11,43,44] The major factor responsible for deviations from eq 2 is the effect of fluid−solid interactions. The physical parameters of nitrogen used in eq 2, which are those for the bulk liquid or a planar infinite surface, cannot be applied to a restricted environment as cylindrical mesopores. The Kelvin equation has been extended to a confined environment by Tolman,[45,46] who derived the following expression for the dependence of the surface tension γ on the radius of curvature of the surface R_K:

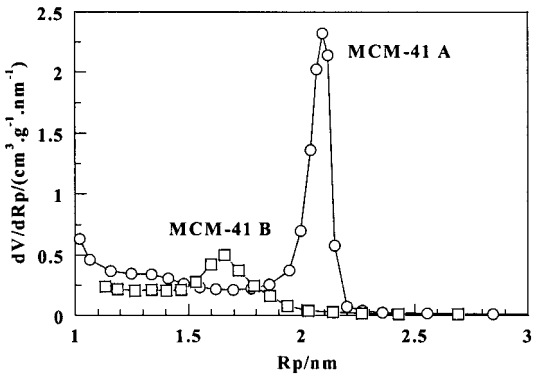

Figure 8. Pore size distributions calculated from the adsorption branch of the nitrogen adsorption isotherms at 77 K on MCM-41 A and B, by using the corrected Kelvin equation.

$$\gamma = \frac{\gamma_\infty}{1 - \frac{2\delta}{R_\mathrm{K}}} \qquad (4)$$

where δ is the thickness of the monolayer of nitrogen adsorbed at the liquid−gas interface. By substituting γ_∞ in eq 2 by the expression taken from eq 4, we obtain the corrected Kelvin equation giving the mesopore radius as a function of the relative pressure:

$$\mathrm{Rp}(p/p_0) = \frac{2\gamma_\infty V_\mathrm{L}}{RT\,Ln(p/p_0)} + 2\delta + t(p/p_0) \qquad (5)$$

Thus, the pore size distribution has been determined by using this equation with $\delta = 0.33$ nm as suggested by Ahn et al.,[47] who found with this empirical value an excellent agreement between the surface tension values measured and those calculated using eq 4.

The values of the mesopore radius (Rp) determined by each method are in very good agreement (Table 1). The deviation between these values never exceeds the scattering of experimental data (pore size distribution, as shown in Figure 8). The mean pore radius of MCM-41 A is close to 2 nm, while the wall thickness is 0.66 nm. This value is similar to those given in the literature for similar materials[32,33,48−51] and corresponds to 2 or 3 silicate layers.

Influence of Aging on the Porosity of MCM-41 A. The adsorption isotherm of nitrogen on the mesoporous silica MCM-41 A aged for 3 months under ambient (temperature and humidity) conditions, MCM-41 B, is shown in Figure 6. Compared to the isotherm of the freshly calcined MCM-41 A, the new isotherm shows a large decrease of the adsorption capacity and an increase of the external surface area of the sample. The shape of the condensation step is less vertical, and it has shifted to lower relative pressures p/p_0, indicating that the pore diameter is reduced while the pore size distribution is more extended (Figure 8). No micropores are detected, as seen from the shape of the t-plot (Figure 7). The values of pore surface area, pore volume, specific surface area,

(42) Gregg, S. T.; Sing, K. S. W. *Adsorption, Surface Area and Porosity*; Academic Press: London, 1982.
(43) Ravikovitch, P. I.; Wei, D.; Chueh, W. T.; Haller, G. L.; Neimark, A. V. *J. Phys. Chem*. **1997**, *101*, 3671.
(44) Neimark, A. V.; Ravikovitch, P. I.; Grün, M.; Schüth, F.; Unger, K. K. *J. Colloid Interface Sci*. **1998**, *207*, 159.
(45) Defay, R.; Prigogine, I. *Surface Tension and Adsorption*; Longmans, Green & Co.: London, 1966.
(46) Tolman, R. C. *J. Chem. Phys*. **1949**, *17*, 333.
(47) Ahn, W. S.; Jhon, M. S.; Pak, H.; Chang, S. *J. Colloid Interface Sci*. **1972**, *38*, 605.
(48) Chen, C. Y.; Li, H. X.; Davis, M. E. *Microporous Mater*. **1993**, *2*, 17.
(49) Feuston, B. P.; Higgins, J. B. *J. Phys. Chem*. **1994**, *98*, 4459.
(50) Stucky, G. D.; Monnier, A.; Schuth, F.; Huo, Q.; Margolese, D.; Kumar, D.; Krishnamurty, M.; Petroff, P.; Firouzi, A.; Janicke, M.; Chmelka, B. F. *Mol. Cryst. Liq. Cryst*. **1994**, *240*, 187.
(51) Kruk, M.; Jaroniec, M.; Ryoo, R.; Kim, J. M. *Microporous Mater*. **1997**, *12*, 93.

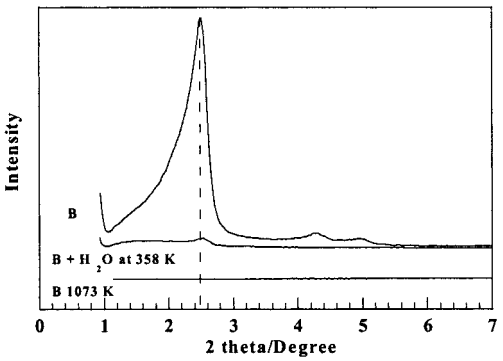

Figure 9. X-ray diffraction patterns of MCM-41 B, after thermal treatment at 1073 K and after hydrothermal treatment at 358 K.

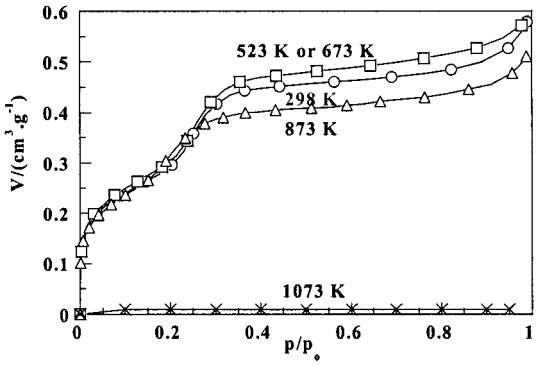

Figure 10. Effect of the activation temperature of MCM-41 B on the adsorption isotherm of N_2 at 77 K.

and pore diameter, derived from this plot (Table 1), are all smaller than those determined for sample A. Despite these differences in pore characteristics between samples A and B, the hexagonal arrangement of the cylindrical pores in sample B is retained, as suggested by the XRD pattern (Figure 9). However, only three diffraction peaks are now well resolved. The broader and less intense reflections than in the case of MCM-41 A may be related to the effect of physically adsorbed water on the XRD intensities but can also reflect a partial collapse of the pore structure during rehydration. The latter hypothesis is supported by the nitrogen adsorption results which indicate that 54% of the pore volume of MCM-41 A was lost during the 3 month period of slow rehydration (by hydrolysis) at room temperature. This value is in line with that of 35% obtained by Zhao et al.[52] for an overnight rehydration of Si−MCM-41 at room temperature. The most important feature that can be noticed on the FTIR spectrum of MCM-41 B diluted in KBr (Figure 5) is the appearance of a shoulder located at 969 cm^{-1}, which can be attributed to Si−OH bending vibrations. This new band and the higher relative intensity of the broad absorption band centered at 3435 cm^{-1} (H-bonded silanol groups) compared to that of the band at 1078 cm^{-1} ($\nu_{Si-O-Si}$) reveal that the amount of Si−OH groups has increased. This clearly suggests that breaking of Si−O−Si bonds through hydrolysis has occurred during aging. Therefore, besides the important modifications in the pore structure, changes in surface chemistry also logically occurred. In addition, a shift of the absorption bands at 1078 cm^{-1} ($\nu_{Si-O-Si}$) and 450 cm^{-1} (ν_{O-Si-O}) to higher wavenumbers was observed for the aged sample. Such a shift can reflect a relaxed constraint in the walls of sample MCM-41 B.

Neither the nitrogen adsorption isotherm nor the XRD pattern of an aliquot of MCM-41-A stored under dry nitrogen for more than 3 months shows any significant change. It is concluded that while the template-free mesoporous MCM-41 materials appear very sensitive to ambient humidity, readily hydrolyze, and undergo a partial structure collapse, the same samples can be stored quasi indefinitely under dry conditions, without any substantial structural damage.

Our results are in line with the recent observations by Landau et al.,[19] who noted that when Si−MCM-41 materials were synthesized at room temperature, they were readily degraded upon calcination and further wetting with neutral water. On the other hand, a further hydrothermal treatment of the same material at high temperature (equivalent to our experimental procedure) markedly improved their thermal stability. Ryoo and Jun[53] also observed such a behavior.

Table 2. Pore Characteristic Values of the MCM-41 Materials (Sample B) after Thermal Treatment under Vacuum at Different Temperatures, As Derived from Nitrogen Adsorption Measurements at 77 K

	temperature		
	298 K	523 K	873 K
$(p/p_0)_{step}$	0.20−0.36	0.20−0.36	0.15−0.32
St/m^2 g^{-1}	585	602	550
Sext/m^2 g^{-1}	48	58	51
Sp/m^2 g^{-1}	537	544	499
Vp/cm^3 g^{-1}	0.418	0.435	0.368
Rp/nm	1.56	1.60	1.47
Rp(K)/nm	1.73	1.75	1.63
< Rp(K) <	1.53−2.11	1.54−2.23	1.42−1.98

Finally, in our case, once MCM-41 A had partially degraded after about 3 months aging, it remains relatively stable, as suggested by the similar nitrogen adsorption isotherms plotted for MCM-41 aged for 3 and 6 months[29] (not shown). This important finding suggests that calcined (and strained) MCM-41 materials are rapidly subject to hydrolysis, which breaks some Si−O−Si bonds and restores a more relaxed and hence stabilized material. The resulting solid would still exhibit mesoporous characteristics sufficient enough for its further utilizations as catalysts or adsorbents.

Thermal Stability. Nitrogen adsorptions were conducted on sample MCM-41 B activated under vacuum at different temperatures (523, 673, 873, and 1073 K) with the aim of studying the thermal stability of MCM-41. The adsorption isotherms are shown in Figure 10, and the pore characteristics of the samples derived from the *t*-method after thermal treatment at 523 and 873 K are given in Table 2. For activation temperatures up to 673 K, no important changes were observed. The pore volume and the specific surface area slightly increase upon the first heating (523 or 673 K) because the water, either adsorbed on the pore walls or stemming from the decomposition of the surface hydroxyl groups, is evacuated during the heating under vacuum. Oppositely, thermal treatments above 673 K lead to a more marked damage of the MCM-41 structure: a decrease of 15% in the adsorption capacity and a shift to lower relative pressures of the condensation step are observed for the sample heated at 873 K (Figure 10). This is consistent with the pore size distribution curve of this sample (Figure 11) that clearly indicates a decrease of the pore radius, estimated at 1.63 nm by the 2*V*/*S* method. If the activation temperature is increased to 1073 K, the porous structure of MCM-41 is

(52) Zhao, X. S.; Audsley, F.; Lu, G. Q. *J. Phys. Chem. B* **1998**, *102*, 4143.

(53) Ryoo, R.; Jun, S. *J. Phys. Chem.* **1997**, *101*, 317.

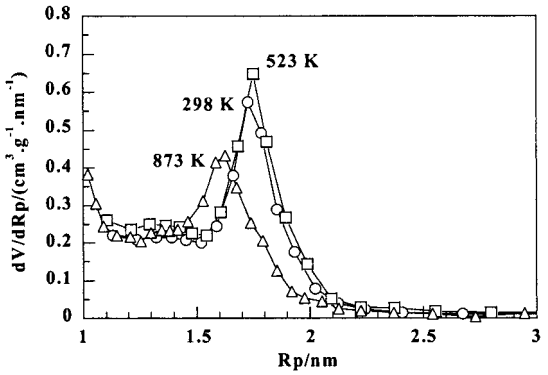

Figure 11. Pore size distribution of MCM-41 B after activation at different temperatures under vacuum.

Table 3. Pore Characteristic Values of the MCM-41 Materials (Sample B) after Uniaxial Compaction under Ambient Conditions and Derived from Nitrogen Adsorption Measurements at 77 K[a]

	compaction pressure			
	0 MPa	100 MPa	500 MPa	1000 MPa
$(p/p_0)_{step}$	0.20−0.36	0.18−0.37	0.21−0.37	0.18−0.38
St/m^2 g^{-1}	602	583	457	392
Sext/m^2 g^{-1}	58	72	57	39
Sp/m^2 g^{-1}	544	511	400	353
Vp/cm^3 g^{-1}	0.435	0.399	0.288	0.215
Rp/nm	1.60	1.56	1.44	1.22
Rp(K)/nm	1.75	1.75	1.75	1.75
< Rp(K) <	1.54−2.23	1.50−2.23	1.53−2.24	1.52−2.05

[a] The samples were activated under vacuum at 523 K prior to each adsorption measurement.

even more affected, as already reported for other pure silica MCM-41 samples prepared by different methods.[23,54] Indeed, the amounts of nitrogen adsorbed on this sample are extremely small. Moreover, the XRD pattern (Figure 9) does not exhibit any diffraction peak in the low-angle region (2−8° 2θ), indicating that the honeycomb structure of MCM-41 B was completely destroyed. It is concluded that the activation temperature has little influence on the porosity of the sample when an aged sample such as MCM-41 B is activated at a temperature at (or lower than) 673 K. In contrast, when the as-synthesized MCM-41 is directly heated in air, it only starts to collapse above 1023 K if it is maintained at that temperature for at least 4 h.[23] This can be easily rationalized if one considers that a freshly calcined sample (MCM-41 A) involving a quasi nondefected network would be less subject to thermal degradation than a framework that was preliminarily fragilized through partial hydrolysis upon aging (sample B). Our results actually show that both the calcination conditions and the nature of the precursor (fresh or aged sample) dramatically influence the final stability of the material.

The IR absorption spectra in the hydroxyl region were recorded for the nontreated sample and the sample activated at 1073 K after rehydration with ambient air moisture (Figures 4 and 5). The decrease of the absorption bands at 1636 and 3700−2700 cm^{-1} is in line with the parallel increase of the hydrophobic character of the material (healing of the Si−OH groups) with the activation temperature. The disappearance of the Si−OH band at 960 cm^{-1} and the shift of the Si−O−Si band at 1093 cm^{-1} with increasing temperature can indeed be explained by a dehydroxylation of the silanol groups leading to the formation of siloxane bridges.[34,53] This phenomenon has been observed in many silica gels.[55] In the particular case of MCM-41 B type materials, this dehydroxylation process first leads to the pore closure and then to the channel collapse, as supported by the shape of the nitrogen adsorption isotherm of the sample activated at 1023 K (Figure 10).

Mechanical Stability. Mechanical properties of hexagonal micelle-templated silicas are also important characteristics to control for their efficient applications as catalysts, catalyst supports, or adsorbents. Such materials can be very fragile under crushing pressure (e.g., during pelletization experiments), especially if the freshly calcined materials are not protected from water.[27,56] Galarneau et al.[25] noted that mechanical and thermal degradations of MCM-41 follow two different mechanisms. In particular, under pressure, the material can be destroyed by zones, some remaining intact and some others being totally crushed. In such a case, the long-distance order is decreasing, with, as a consequence, a parallel decrease in intensity of the main XRD peaks, while the cell parameters remain unchanged. Wu et al.[24] note that the macroscopic order of MCM-type materials can be retained even if they are submitted to a uniaxial compression of about 12 GPa and that the slight pressure-induced distortions are reversible.

Here, we are checking the effect of a uniaxial compaction on both the ordered pore structure of MCM-41 B and the subsequent decrease of the adsorption properties of the material in the medium-pressure range (below 1 GPa). About 7 mg of MCM-41 B sample was compressed in a steel die of 12.9 mm diameter, using a hand-operated press, for 1 min, under ambient conditions. The sample was compressed to 100, 500, and 1000 MPa. Not less than 20 wafers were thus required to perform a nitrogen adsorption experiment. The wafers were broken up in order to avoid diffusion problems.

The nitrogen adsorption isotherms indicate that the compression of MCM-41 at 100 MPa did not involve important changes in the pore volume of the material since it is only 8% lower than that of the noncompressed sample. The pore surface area and the external surface area determined from the *t*-plot were also slightly modified by this compression (Table 3). These features prove that MCM-41, once aged for 3 months and stabilized, can withstand a 100 MPa uniaxial pressure without undergoing too much damage. Nevertheless, if the applied pressure is increased to 1000 MPa, a severe decrease in the adsorption capacity, specific surface area, and pore radius is observed. The isotherm clearly shows that the sample underwent drastic damage since the pore-filling step is barely visible (Figure 12). It is therefore obvious that almost no detectable mesopores can be found for the 1000 MPa compacted sample compared with the parent sample MCM-41 B. On the pore size distribution curves, the portion of mesopores is reduced while the average pore radius remains unchanged with increasing applied pressure (Figure 13). This result suggests that a part of the mesopores is destroyed by mechanical compression and that the portion of destroyed mesopores increases with the compaction pressure. This can be explained by a nonhomogeneous compression of the powder, meaning that some particles are compacted enough to be destroyed whereas others remain intact. Another explanation consists of assuming that only pores surrounded by defected walls (hydrolysis of Si−O−Si bonds upon aging) are

(54) Chen, C. S.; Kawi, S. *J. Phys. Chem. B* **1999**, *103*, 8870.
(55) Morishige, K.; Fujii, H.; Uga, M.; Kinikawa, D. *Langmuir* **1997**, *13*, 3494.
(56) Koyano, K. A.; Tatsumi, T.; Tanaka, Y.; Nakata, S. *J. Phys. Chem. B* **1997**, *101*, 9436.

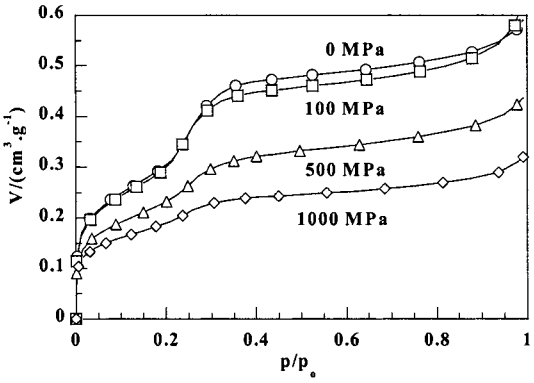

Figure 12. Effect of the compaction pressure on the adsorption isotherm of N_2 at 77 K of MCM-41 B.

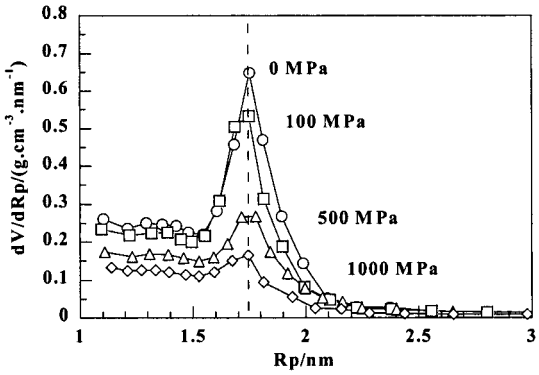

Figure 13. Pore size distribution of MCM-41 B after uniaxial compaction under different pressures by using the corrected Kelvin equation.

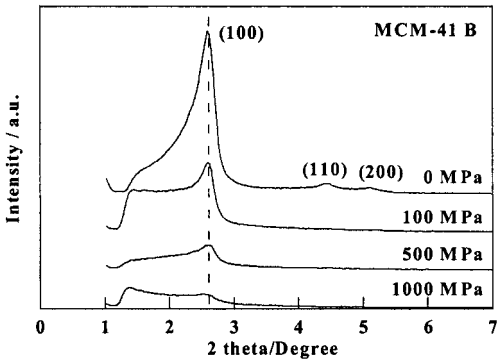

Figure 14. X-ray diffraction patterns of MCM-41 B, after uniaxial compaction under different pressures.

affected by compression; the more defected the walls, the more fragile the corresponding pores, following the mechanism proposed by Galarneau et al.[25] A partial destruction of the mesopores is confirmed by the XRD patterns shown in Figure 14. The decrease in intensity of the (100) peak without shift toward lower or higher angles with increasing pressure means that the amount of mesopores decreases but their sizes remain unchanged. The shoulder that appears on the left side of the (100) peak is attributed to the presence of secondary mesopores. This shoulder is also logically observed on the noncompacted MCM-41 B, in which the structure is also partly destroyed. As the compaction pressure increases, the mesopores are progressively destroyed, leading to a decrease in the total porous volume and specific surface area, while these secondary mesopores do not seem to be affected by the mechanical treatment.

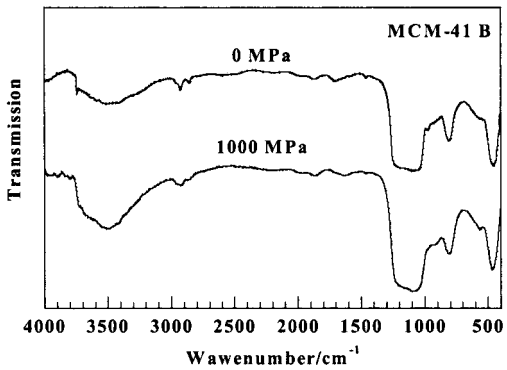

Figure 15. FTIR spectra in the 4000−400 cm^{-1} region of MCM-41 B before and after uniaxial compaction under a pressure of 1000 MPa.

Our results are in very good agreement with the recent works of Tatsumi et al.,[57] who also found that the mesoporosity of MCM-48 and MCM-41 materials underwent severe damage by mechanical compression. Moreover, they showed that the effect of compaction is strongly dependent on the degree of hydration of the material, which is in line with our second explanation. Indeed, these authors also assume that the loss of mesoporosity would be the result of a mechanochemical hydrolysis of Si−O−Si bonds to yield Si−OH groups. They also claim that hydrolysis would be easier when the solid is strained by mechanical compression. Ryoo et al.[53] have also shown that siloxanes, when strained upon calcination in the presence of water, are further more readily hydrolyzed in contact with water than unstrained siloxanes. In our case, however, no important modifications of the Si−O−Si and Si−OH bands were observed on the IR spectra after compaction (Figure 15). This is not surprising taking into account that the aged sample has already been substantially hydrolyzed and that FTIR would only probe bonds independently on their surrounding mesopores. However, a very slight increase in intensity of the bands at 960 and 3500 cm^{-1} assigned to silanols groups may be discerned. This seems to confirm that the hydrolysis of the siloxane bonds is easier when the material is strained.

Hydrothermal Stability. After calcination, MCM-41 B was submitted to a saturating water vapor pressure at 358 K in a desiccator for 3 weeks. The porous structure of the sample was then characterized by nitrogen adsorption and X-ray diffraction. The corresponding isotherm is shown in Figure 6 with that of the original material for comparison. The hydrated sample isotherm exhibits not a usual type IV shape but a type II shape in the IUPAC classification. The type II isotherm is typical of the adsorption on a nonporous solid. Moreover, the XRD pattern presents only a very weak reflection at low angles, indicating that a poorly ordered material is obtained after hydrothermal treatment (Figure 9). The specific surface area of this material was found dropped down to about 120 $m^2\ g^{-1}$. These results clearly show that important structural changes have occurred during the hydrothermal treatment leading to a nonporous material.[19,58] This loss of porosity arises from the complete hydrolysis of the siloxane bonds that leads to the collapse of the whole mesoporous structure with the resulting material involving a very defected (hydrolyzed) structure, as ascertained by FTIR.[29]

(57) Tatsumi, T.; Koyano, K. A.; Tanaka, Y.; Nakata, S. *J. Porous Mater.* **1999**, *6*, 13.

(58) Ribeiro Carrott, M. M. L.; Esteveao Candeias, A. J.; Carrott, P. J. M.; Unger, K. K. *Langmuir* **1999**, *15*, 8895.

Conclusion

The pore size of MCM-41 materials can be evaluated with a good accuracy from nitrogen adsorption data by using simple models as BET theory, *t*-method, or Kelvin equation. Such models can be applied provided one carefully selects the physical characteristics of the nitrogen molecular probe and takes into account the characteristics of both the solid and the sorbate, such as the hydroxylation state of the surface on the cross-sectional area, the curvature dependence on the surface tension, and the compression of the fluid phase which takes place after condensation in the mesopores.

Although MCM-41 is currently considered ideal as a material of great interest for applications in adsorption and catalysis because of its cylindrical mesopores easily accessible to large molecules and because of its narrow pore size distribution and its very large surface area, our work nevertheless underlines that its field of application can be substantially reduced because of its low stability under usual application conditions. Indeed, after calcination, the mesoporosity of MCM-41 is affected during aging under ambient conditions. However, when synthesized under hydrothermal conditions at high temperature and further calcined, after a preliminary partial destruction upon a medium−long aging period (a couple of months of storage in ambient conditions), the material can become stable while still keeping a substantial mesoporosity. However, upon outgassing in a vacuum above 673 K, the porosity of the aged material can undergo important damage and the solid becomes then very sensitive to moisture (hydrolysis of the siloxane groups) even at low temperature. These poor thermal and hydrothermal stabilities are severe limitations in using such materials in catalysis or adsorption processes, such as hydrocracking or moist air purification. In this last case, for example, regeneration of the adsorbent by heating or by means of water vapor flow is not conceivable.

Finally, care should be taken when subjecting this material to high pressures in applications such as pelletization for IR spectroscopic studies, chromatographic column packing, or extrusion along with a binder, for applications in industrial processes. Water removal from the material followed by a further protection of its surface from water with a monolayer of silane molecules[56] would by far improve the resistance of MCM-41 to mechanical or thermal constraints. In practice, however, it can be easier to prevent extensive hydrolysis of the MCM-41 framework by storing the freshly prepared material in its as-synthesized form or, if the surfactant molecules have to be removed, by storing the calcined form in a dry atmosphere.

LA0118255